Time-Resolved Investigations of Heterobimetallic Cofactor Assembly in R2lox Reveal Distinct Mn/Fe Intermediates

Effie K. Miller,[b] Nicholas E. Trivelas,[a] Pearson T. Maugeri,[c] Elizabeth J. Blaesi,[d] and Hannah S. Shafaat[a,b,c]*

[a]Department of Chemistry and Biochemistry, [b]The Ohio State Biochemistry Program, and [c]The Ohio State Biophysics Program, The Ohio State University, Columbus, OH 43210, USA.

[d]Department of Chemistry, The Pennsylvania State University, University Park, PA 16802, USA.

Supporting Information

Table of Contents

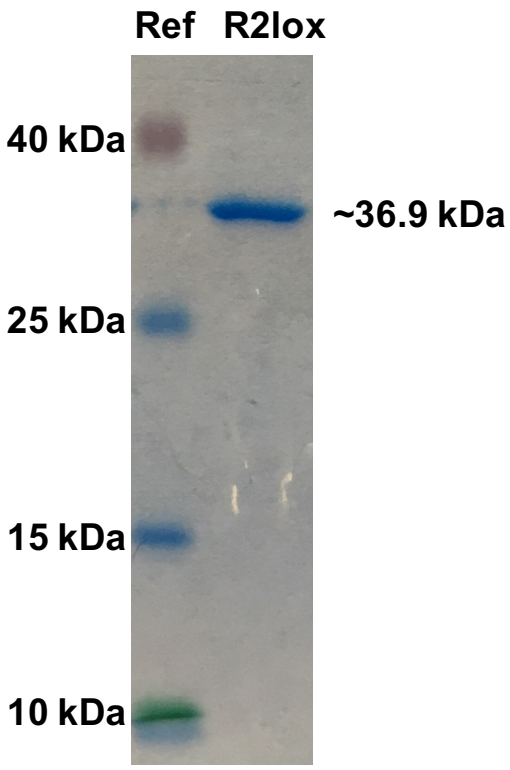

Figure S1. 12% SDS-PAGE of WT *Gk* R2loxI referenced against Spectra Multicolor low range protein ladder (Thermo Fisher Scientific).

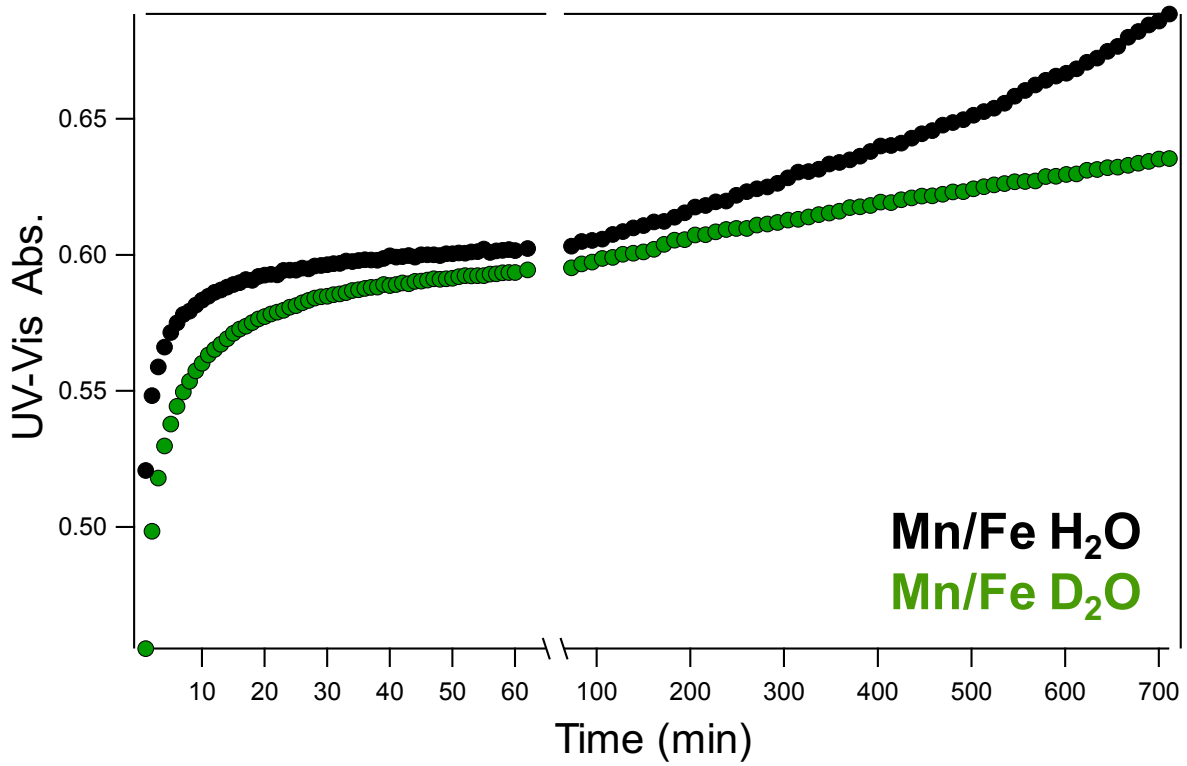

Figure S2. Long-term monitoring of UV-Vis reconstitutions. Stoichiometric Mn/Fe reconstitutions were performed in both protiated and deuterated buffers and monitored over ~12 hours to resolve complete cofactor stabilization. Data from 1-60 minutes were collected at the standard rate of one data point/minute. After the initial 60 minute period, spectra were taken every 10 minutes, with approximately 1 minute required to obtain each spectrum, resulting in a total of 11 minutes represented per data point. Sample absorbance appeared to level out prior to 2 hours; however, continued incubation showed increasing absorbance. This long-term absorbance increase in both samples was attributed to oxidation of excess Fe^{II} in solution. This agrees with previous work, which demonstrates quantitative metallation does not always occur in Mn/Fe R2lox.[1]

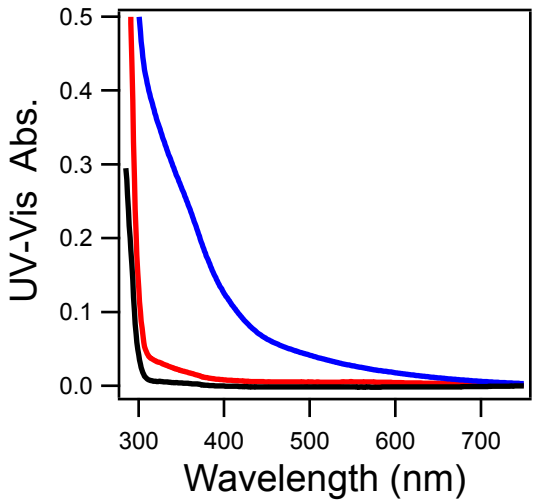

Figure S3. Evidence of weak divalent metal binding in R2lox. Optical spectra of 100 μM apo-R2lox (black); 100 μM apo-R2lox + 1 equiv. Mn^{II} + 1 equiv. Fe^{II} prepared under anaerobic conditions and activated by addition of oxygenated buffer (blue); and 100 μM apo-R2lox + 1 equiv. Mn^{II} + 1 equiv. Fe^{II} prepared under anaerobic conditions, with excess metal ions removed *via* desalting column prior to activation by addition of oxygenated buffer (red), as per the methodology of Bollinger, Krebs, and coworkers.[2] Only low yields of reconstituted protein (< 10%) are observed following desalting. Using the previously reported ε_{350} = 3000 M^{-1} cm^{-1}, a K_D for metal binding of approximately 0.1-1 mM is estimated.[3]

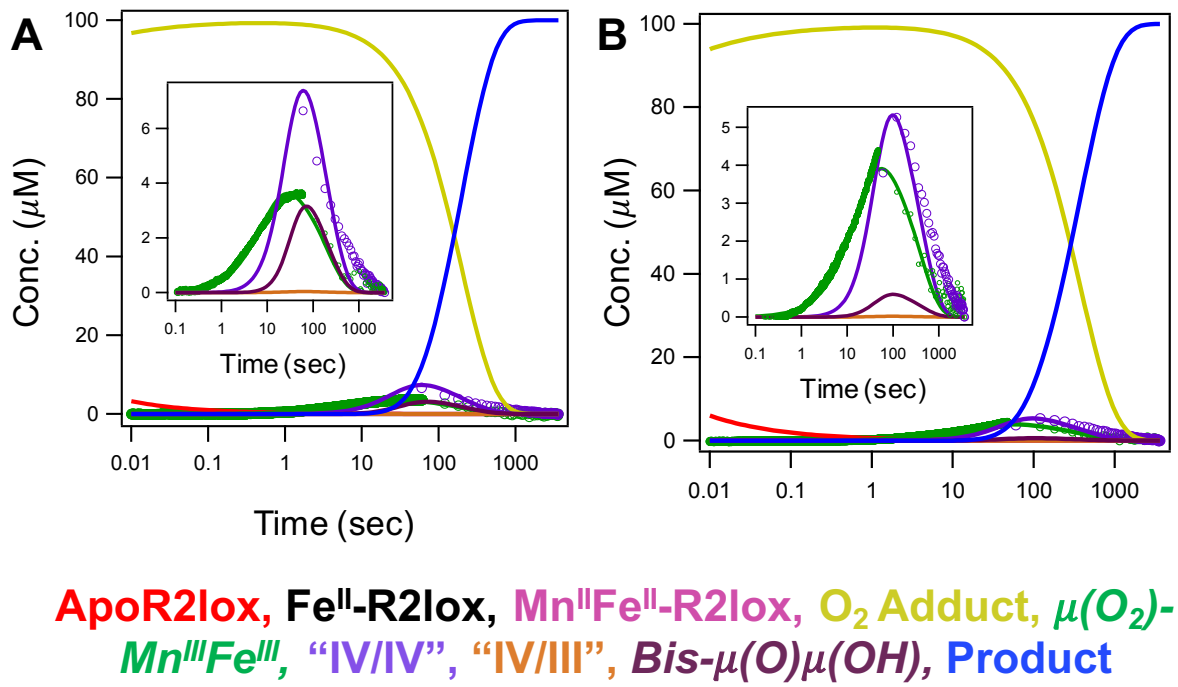

Figure S4. Graphical representation of R2lox reaction model as portrayed by KinTek software (v.6.0), developed from reaction steps outlined in Materials and Methods. Assembly and maturation of Mn/Fe R2lox is modeled based on data obtained in both (A) protiated and (B) deuterated buffers. The Mn binding site (Site 1) is crystallographically disordered in apo-R2lox and only becomes ordered upon Fe binding in Site 2; therefore, Fe binding in Site 2 is thought to occur first. Because stoichiometric amounts of each metal were included in the experiments, the kinetic model is independent of metal binding order. Work is currently underway to experimentally determine order of metal binding.

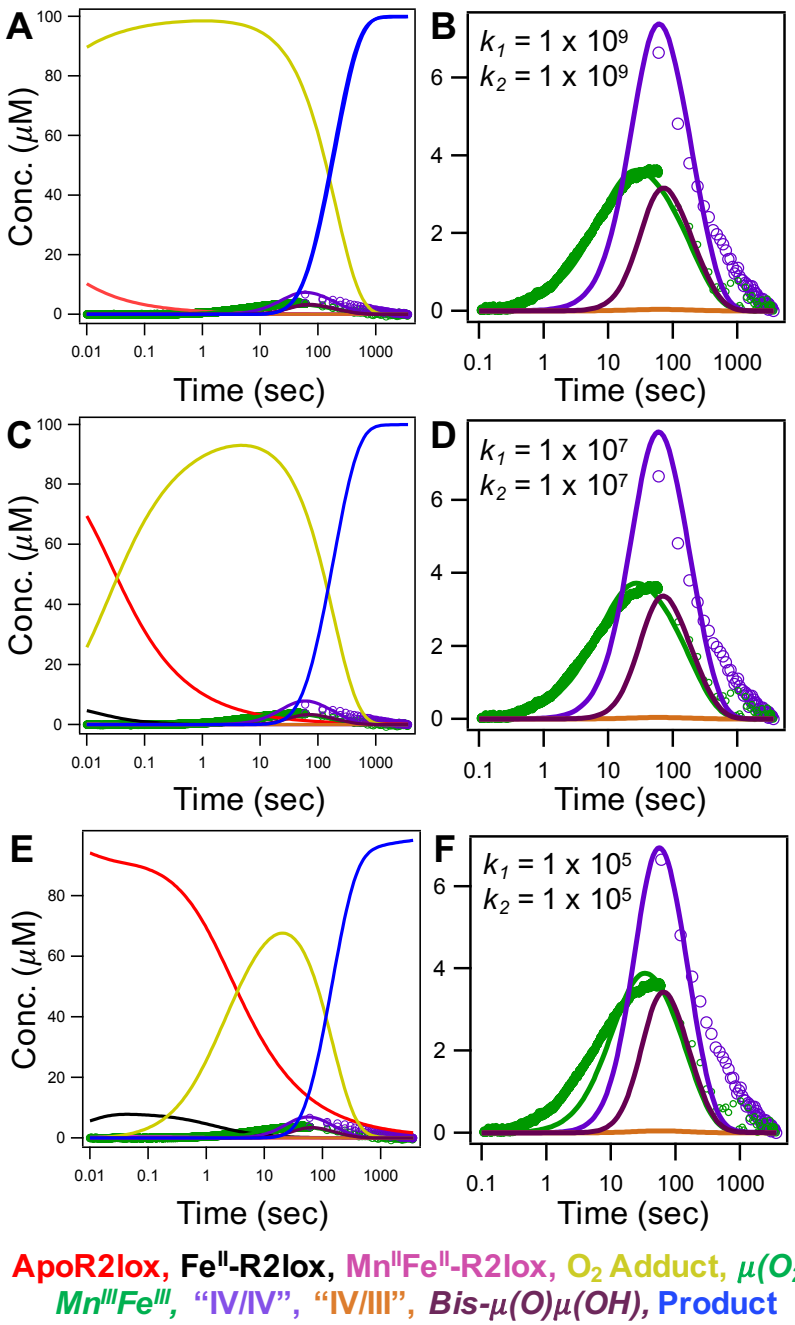

Figure S5. Changes in reaction model as rates of metal binding and O_2 access are adjusted. At rates slower than $1x10^7$ a good fit of the model to the data was not attainable; however, models using values of $1x10^7$ and $1x10^9$ for k_1 produced fits comparable with those of the diffusion-limited model (Table S1).

Table S1. Rate constants from fitting[a] kinetic model to protiated (black) or deuterated (green) experiment data at various rates of metal binding and O_2 access to active site

$k_{1,2}$	k_3 (min^{-1})	k_4 (min^{-1})	k_5 (min^{-1})[b]	k_7 (min^{-1})[c]
1 x 10^{10} M^{-1} s^{-1}	0.30 ± 0.02	7.20 ± 0.45	3.12 ± 1.15	7.20 ± 0.74
1 x 10^{10} M^{-1} s^{-1}	0.159 ± 0.001	3.504 ± 0.034	2.400 ± 0.217	N/A
1 x 10^{9} M^{-1} s^{-1}	0.30 ± 0.03	7.20 ± 0.36	3.12	7.20 ± 5.89
1 x 10^{7} M^{-1} s^{-1}	0.33 ± 0.17	7.50 ± 1.89	3.12	7.20
1 x 10^{5} M^{-1} s^{-1}	0.73	8.10	4.20	8.40

[a]Rates given without standard error represent values which were manually determined during fitting

[b]UV-Vis data for decay of the high-valent intermediate likely contained background signal from metal-oxo absorbance and values for k_5 were held under slower conditions

[c]Rates for product formation were held in models with $k_{1,2}$ slower than $1x10^9$, as lack of data for intermediates prior to product formation made fitting more difficult.

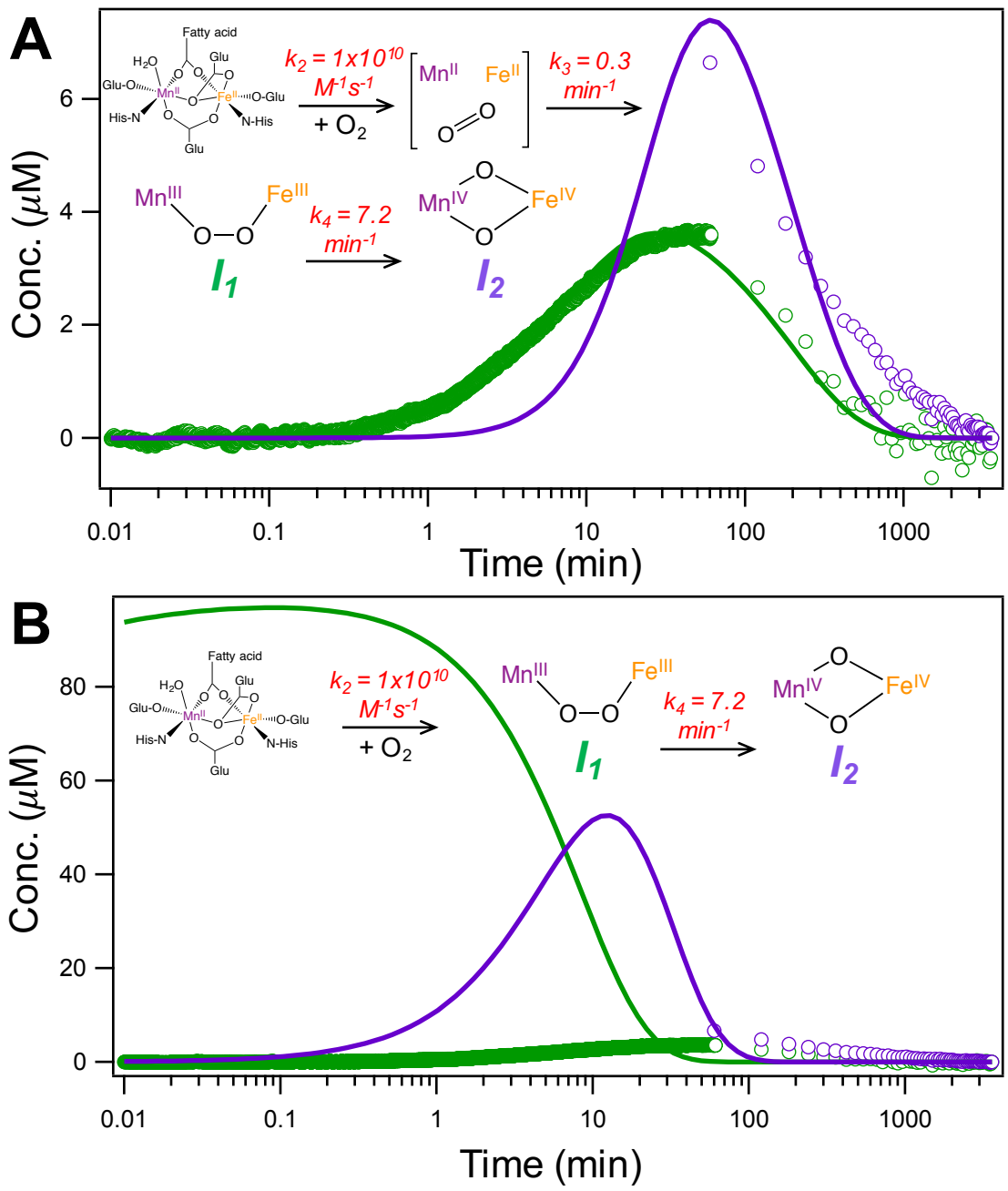

Figure S6. Justification for conformationally gated reaction of O_2 with metals. KinTek model showing formation of I_1 under diffusion-limited conditions considering (*A*) a slow conformational step following O_2 addition to the protein and (*B*) direct, diffusion-controlled O_2 binding to the metal centers. In the case of (B), high concentrations of I_1 would be expected and formation would not be resolved, a significant departure from experimental observations. The depicted O_2-adduct likely resembles the "O" state of sMMO.[4]

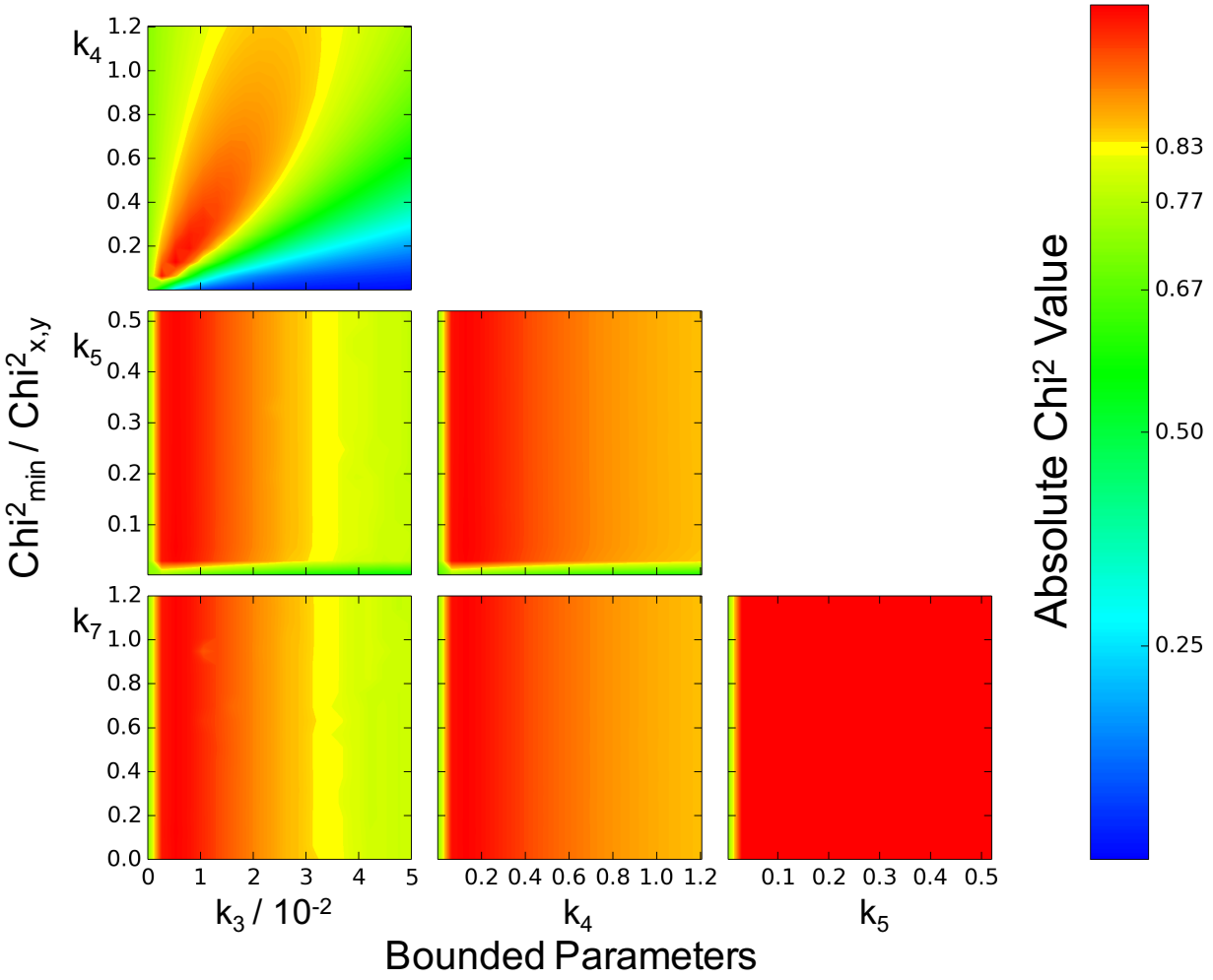

Figure S7. 2D FitSpace analysis on overall fit of kinetic model utilizing built-in KinTek routines. Chi^2 threshold was set to 0.7143 with k_3, k_4, k_5, k_7, allowed to vary. Absolute chi^2 value scale illustrates the location of parameter bounds. These boundaries are defined by examining parameter values in all the possible pair-wise combinations between two parameters, specifically where they can co-vary and produce a good fit. Based on this analysis, k_3 is the best constrained, with previous fitted values for k_4 and k_5 consisting of the upper boundary for these parameters. Product formation (k_7) is the least constrained with minimal bounds.

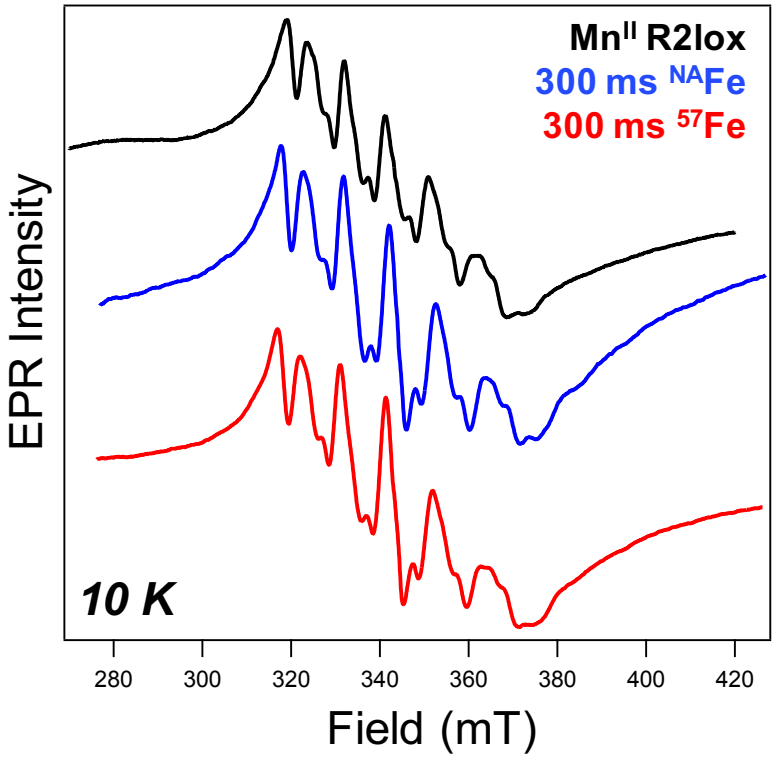

Figure S8. CW X-band EPR spectra of Mn^{II}-only R2lox (black) compared to 300 ms RFQ samples prepared with ^{NA}Fe (blue) and ^{57}Fe (red).

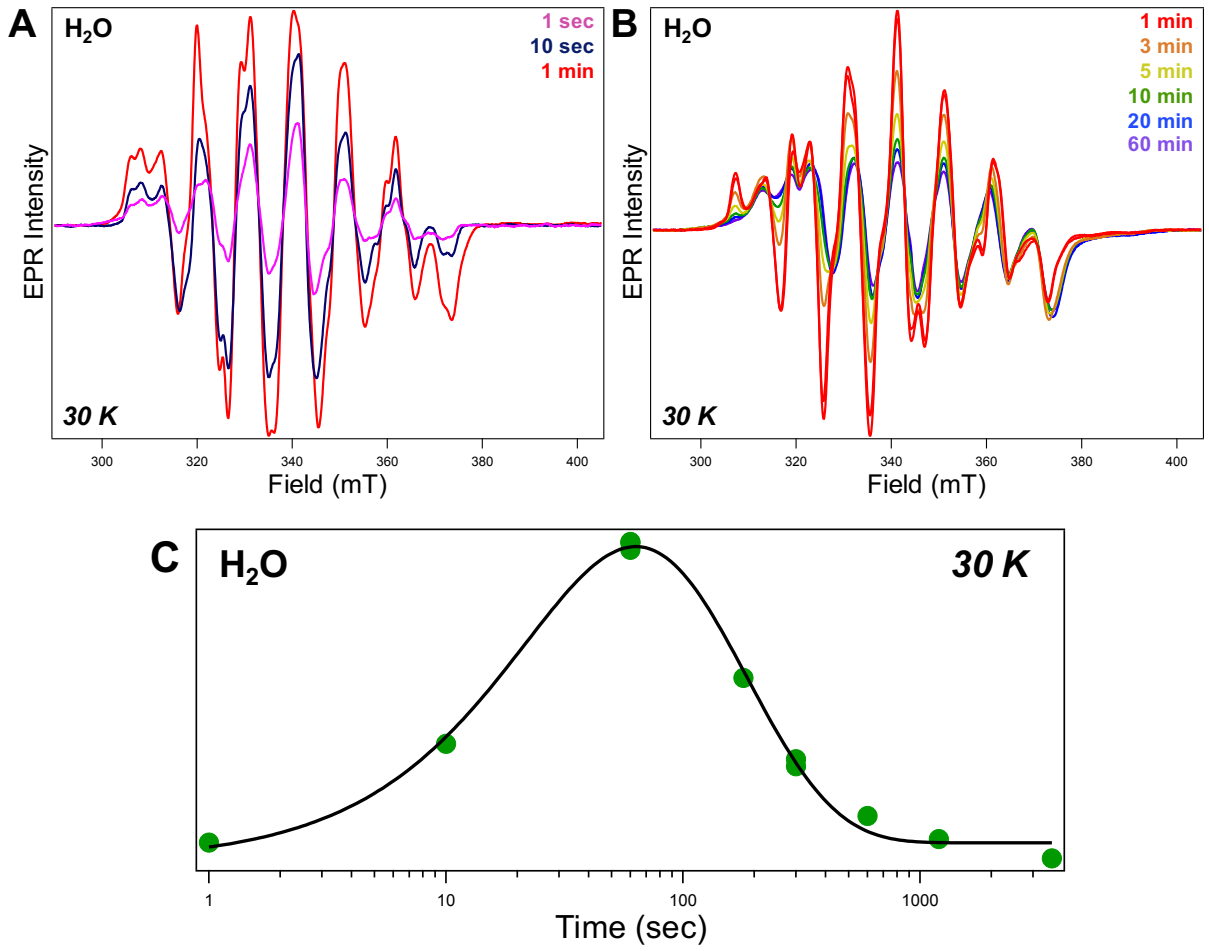

Figure S9. (A) Formation and (B) decay of I_1 monitored at 30 K. Due to experimental constraints, ^{57}Fe RFQ samples were measured in (A), while ^{NA}Fe HQ samples are shown in (B). Intermediate formation and decay monitored at ~307 mT with best fit to double exponential shown (C).

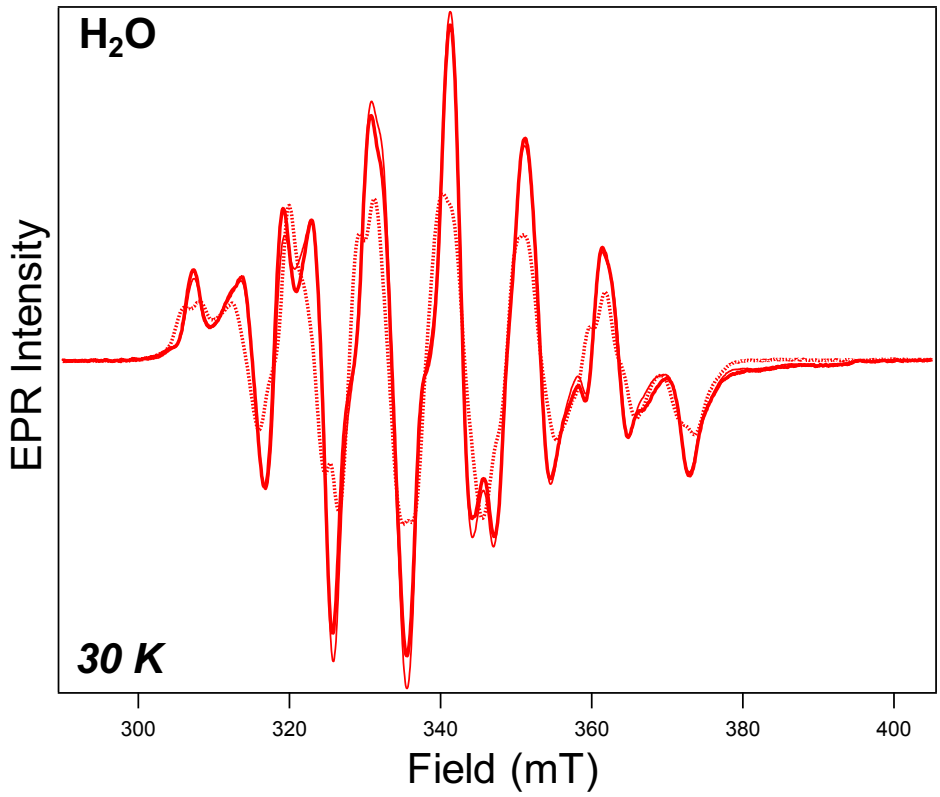

Figure S10. CW X-band EPR spectra of RFQ sample prepared with ^{NA}Fe (thick line), RFQ sample prepared with ^{57}Fe (dotted line), and HQ sample prepared with ^{NA}Fe (thin line), all quenched at t = 1 min and measured at 30 K.

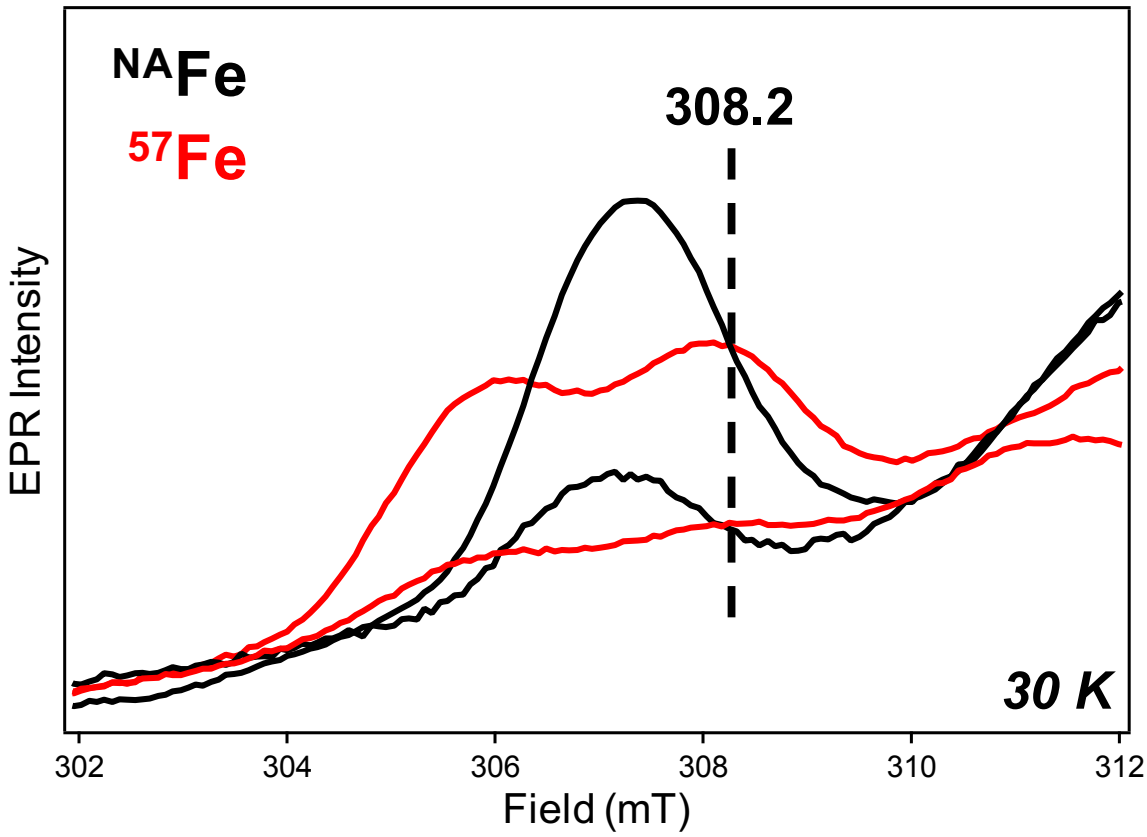

Figure S11. Isosbestic point used in I_1 analysis.

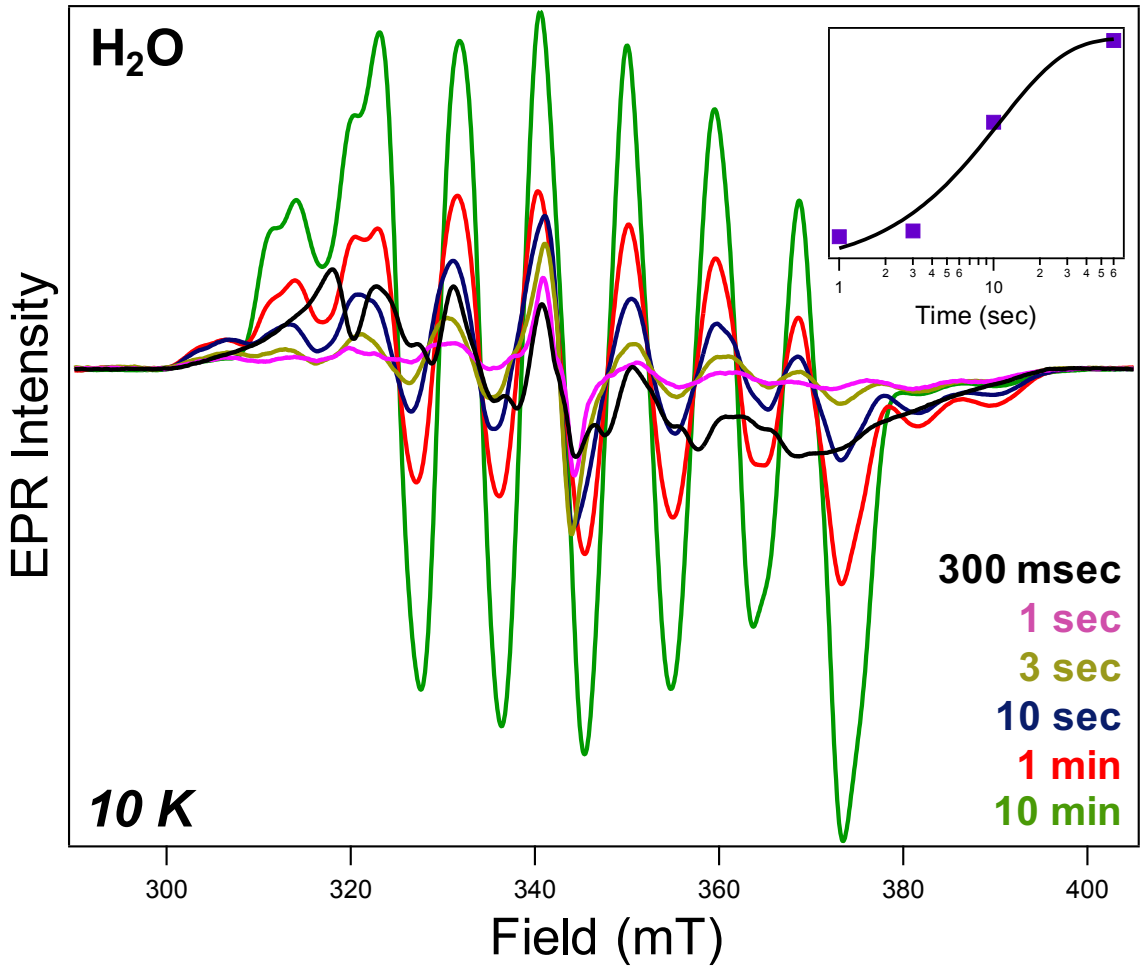

Figure S12. Formation of I_2 monitored at 10 K, using RFQ samples prepared with ^{57}Fe, *(inset)* kinetics of formation monitored at ~390 mT from 1 sec – 1 min with best fit to single exponential shown.

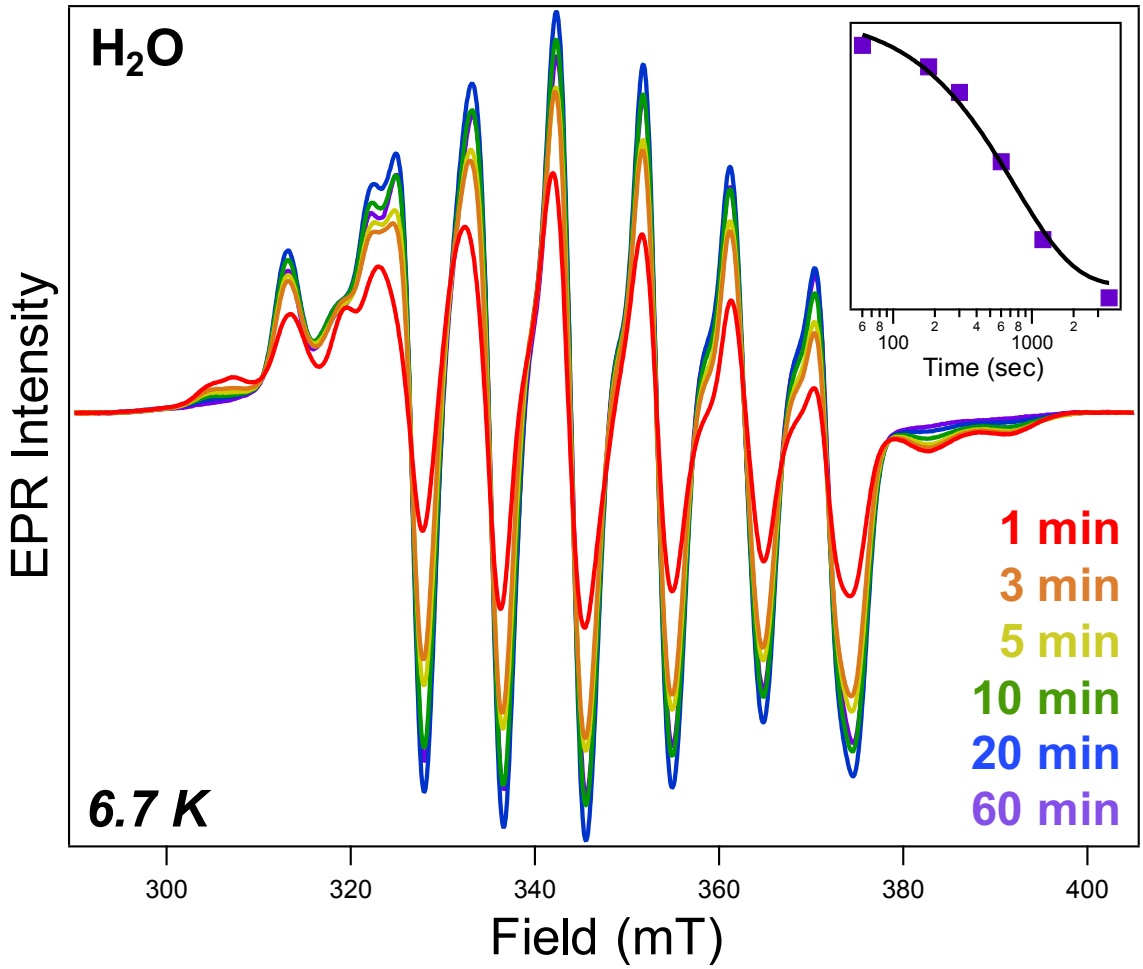

Figure S13. Decay of I_2 monitored at 6.7 K. For 1 min and 5 min timepoints, spectra of ^{NA}Fe HQ samples are shown, *(inset)* kinetics of decay monitored at ~390 mT from 1 min – 60 min with best fit to single exponential shown.

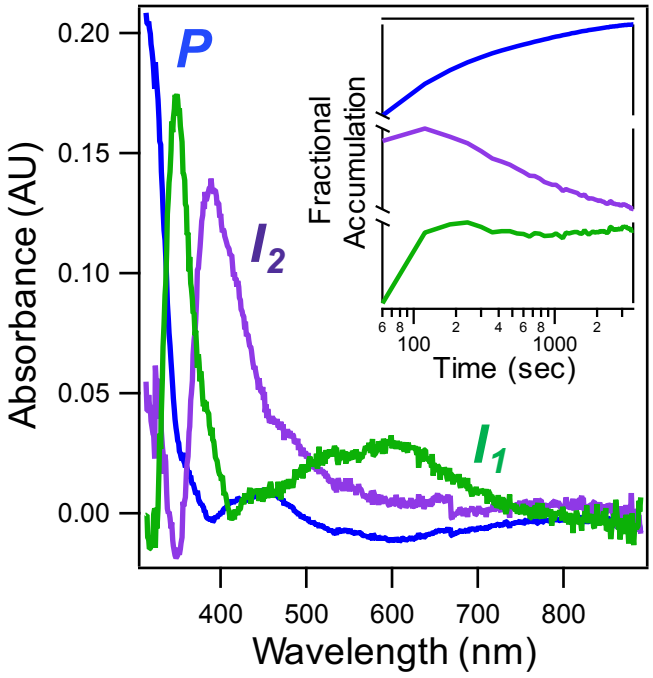

Figure S14. Postulated absorption spectra and concentration profiles of singular value decomposition (SVD) on Mn/Fe R2lox assembly in deuterated buffer.

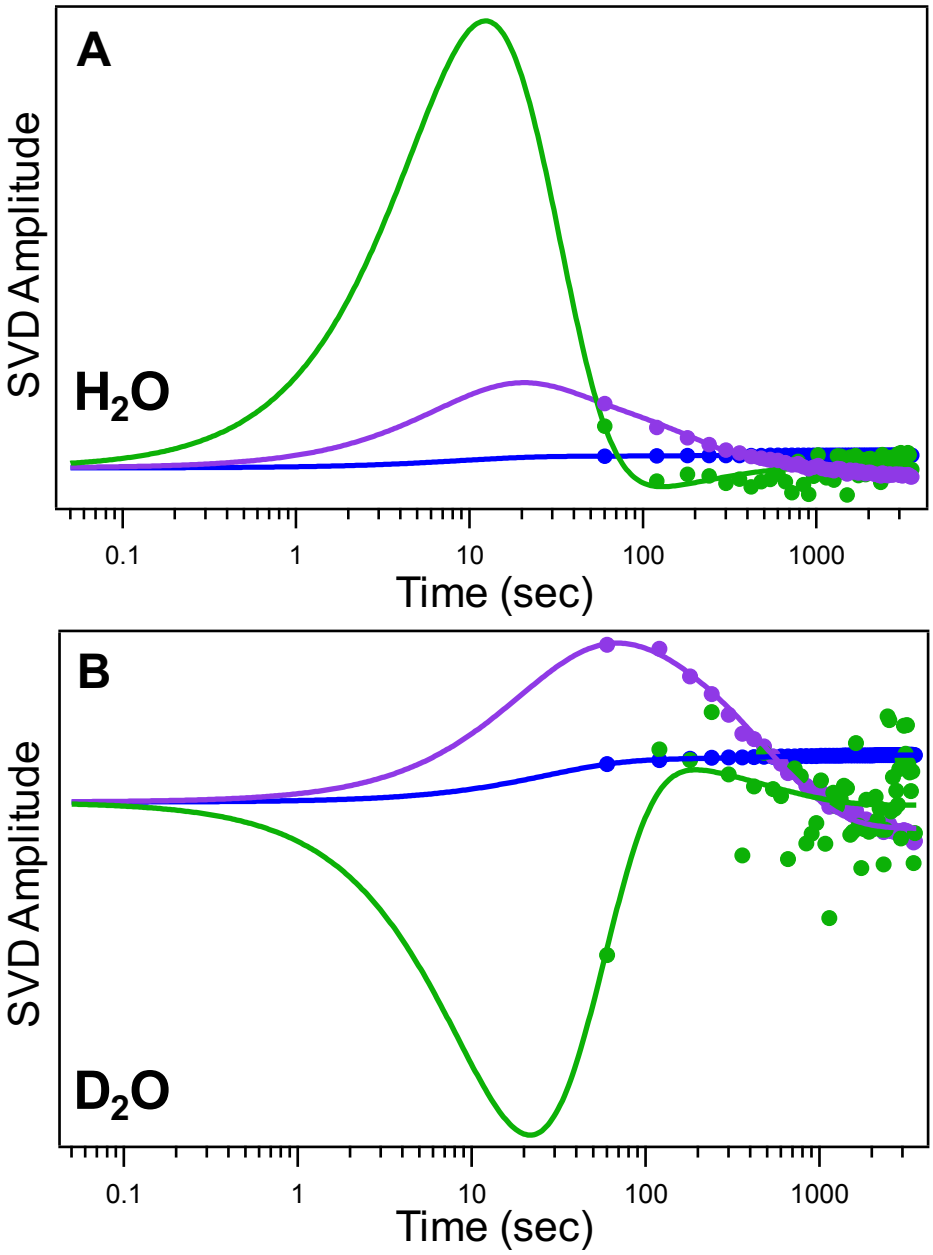

Figure S15. Overlay of SVD amplitudes representing I_1 (green) I_2 (purple) and product (blue) with experimental observables as a global analysis. Good agreement is shown in both protiated (*top*) and deuterated (*bottom*) solvent data sets.

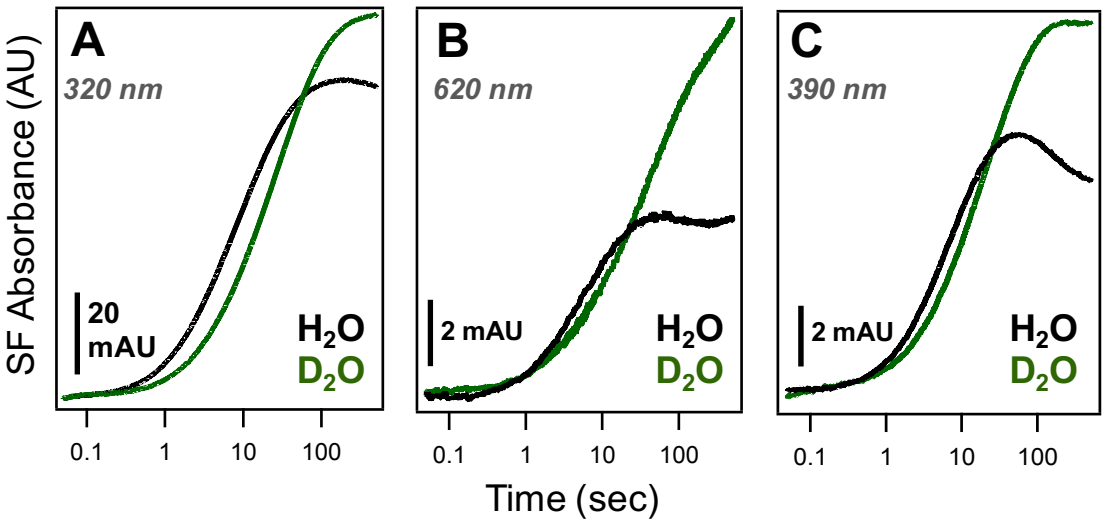

Figure S16. SF-Abs of Mn/Fe R2lox in both protiated (black) and deuterated (green) buffers. (A – B) Product and I_1 formation monitored at 320 nm and 620 nm, respectively. (C) I_2 formation in deuterated buffer monitored at 390 nm. Slight formation KIEs are observed in intermediates, with a more pronounced overall KIE for formation evident in product.

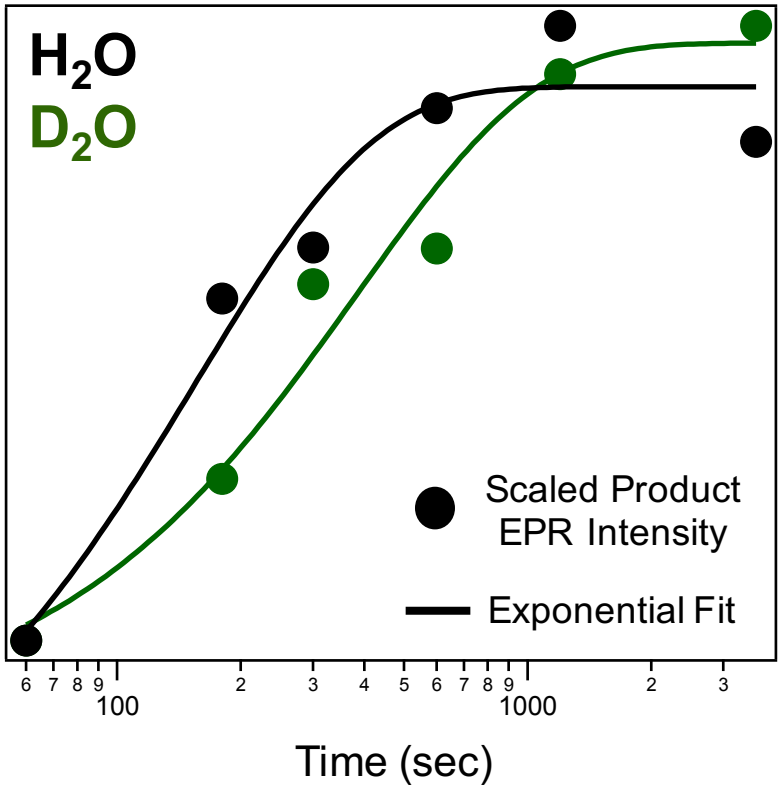

Figure S17. Product formation in protiated and deuterated solvent experiments monitored by change in EPR intensity. Single-exponential fits of the data result in an apparent $KIE_{product}$ ~2.4, with $k_{7,\ protiated} = 0.38\ min^{-1}$ and $k_{7,\ deuterated} = 0.16\ min^{-1}$.

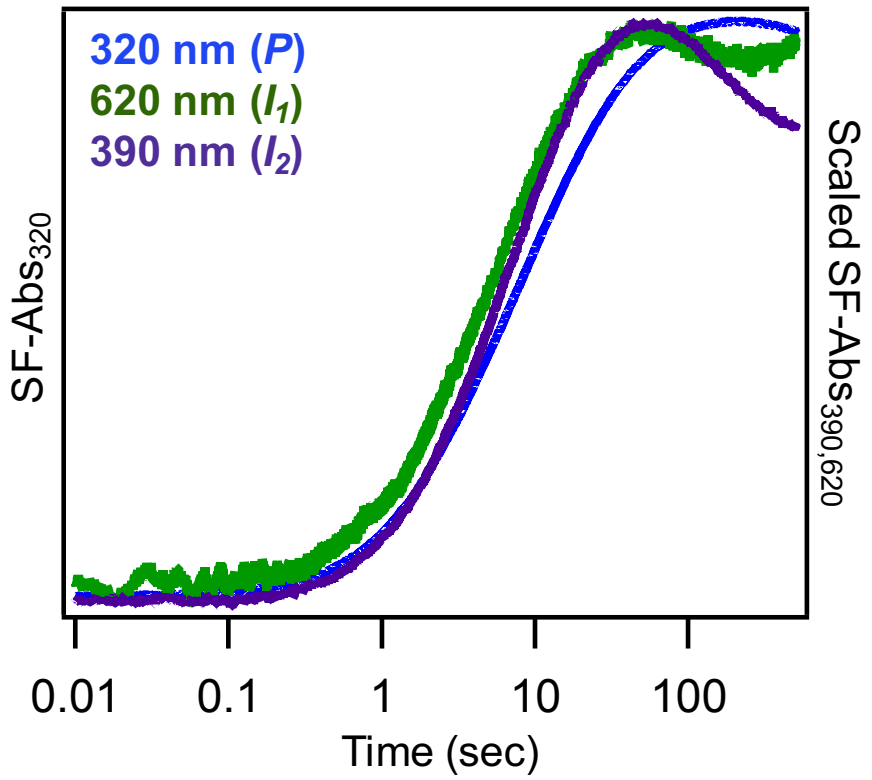

Figure S18. Normalized SF-Abs for 100 μM apo-R2lox + 1 equiv. Mn^{II} + 1 equiv. Fe^{II} in aerated buffer at 620 nm, 390 nm, and 320 nm. Absorbance of I_1 and I_2 precedes product formation, and both intermediates show maximum absorbance at ~40 sec.

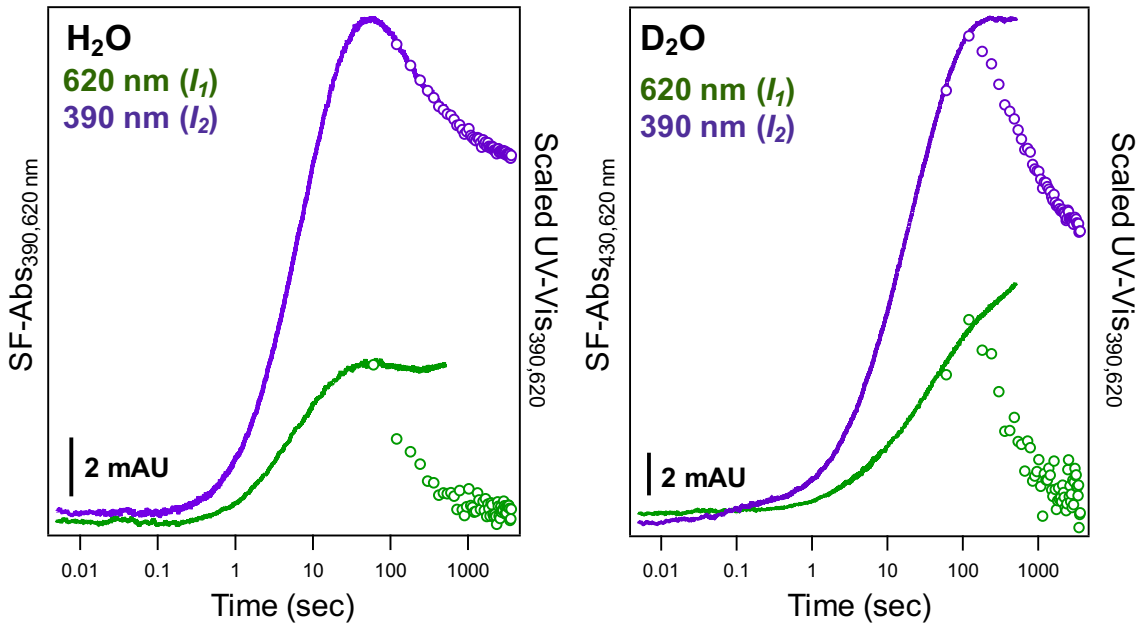

Figure S19. SF-Abs (solid lines) of 100 μM apo-R2lox + 1 equiv. Mn^{II} + 1 equiv. Fe^{II} in aerated protiated (*left*) and deuterated (*right*) buffer. Data are overlaid with scaled UV-Vis absorbance values (open circles) from reconstitution data, showing moderate agreement between measurement methods with widely different mixing technique. Lack of defined peaks in D_2O is attributed to increased precipitation of either Fe^{II} or protein over extended times, as R2lox is less stable in D_2O.

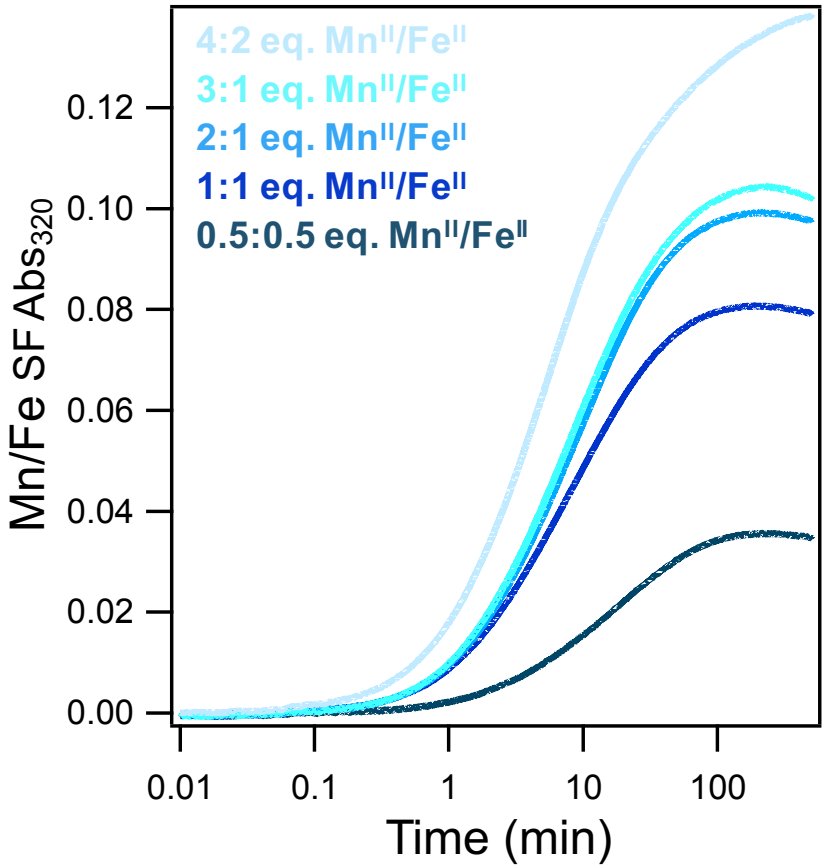

Figure S20. Metal titrations of Mn/Fe R2lox. Metal concentrations were increased in Mn/Fe SF-Abs experiments in an attempt to achieve pseudo-second order kinetic conditions. With the addition of greater than stoichiometric amounts of Fe^{II} (e.g., 4:2 Mn:Fe), product formation appears to continue to increase over long times.

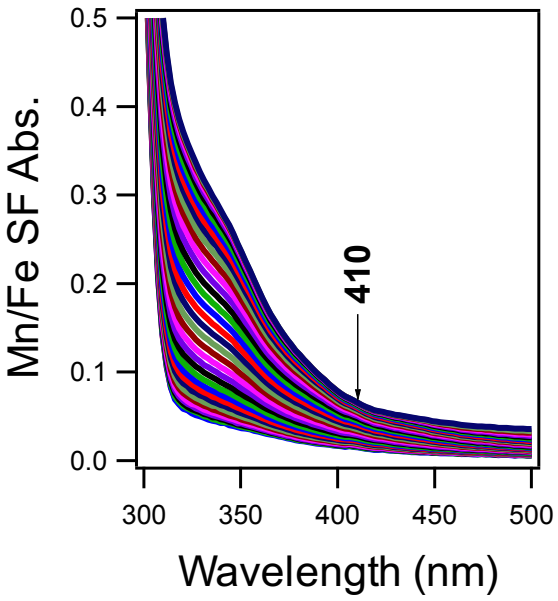

Figure S21. Diode-array SF-Abs of Mn/Fe R2lox. Apo-R2lox was mixed with 1 equivalent of Mn^{II} and Fe^{II} in aerobic buffer. Traces were collected using logarithmic time spacing for a period of 500 seconds; every 20th trace collected is shown. The absence of a sharp peak at 410 nm indicates an absence of the proposed tyrosyl radical under the experimental conditions,[5,6] though rapid decay of such a species may also preclude intermediate accumulation. As mentioned in the text, photodegradation of the sample by multiwavelength light prevented quantitative analysis of intermediate formation; however, qualitative analysis agrees with the single-wavelength data.

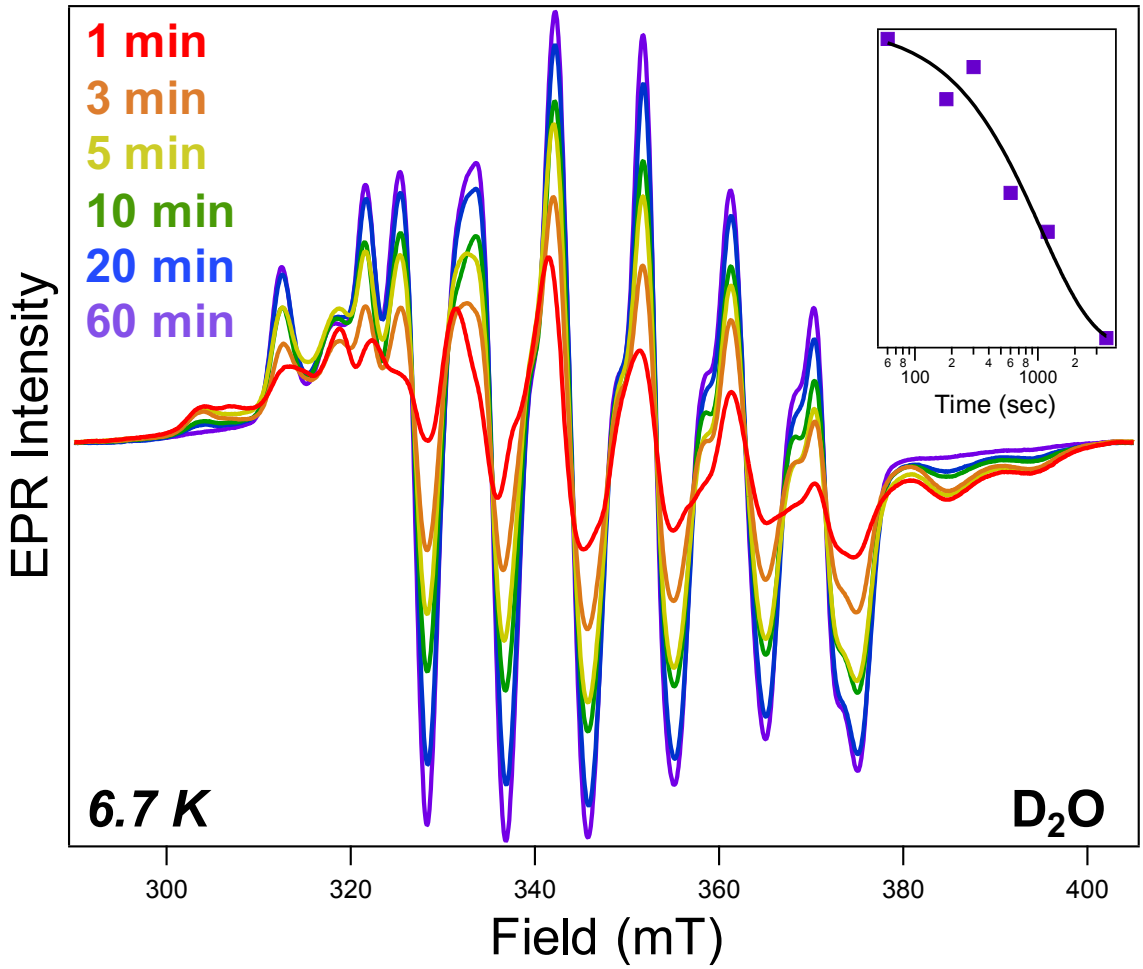

Figure S22. Decay of I_2 in deuterated buffer collected at 6.7 K, *(inset)* kinetics of decay monitored at ~394 mT with best fit to single exponential shown.

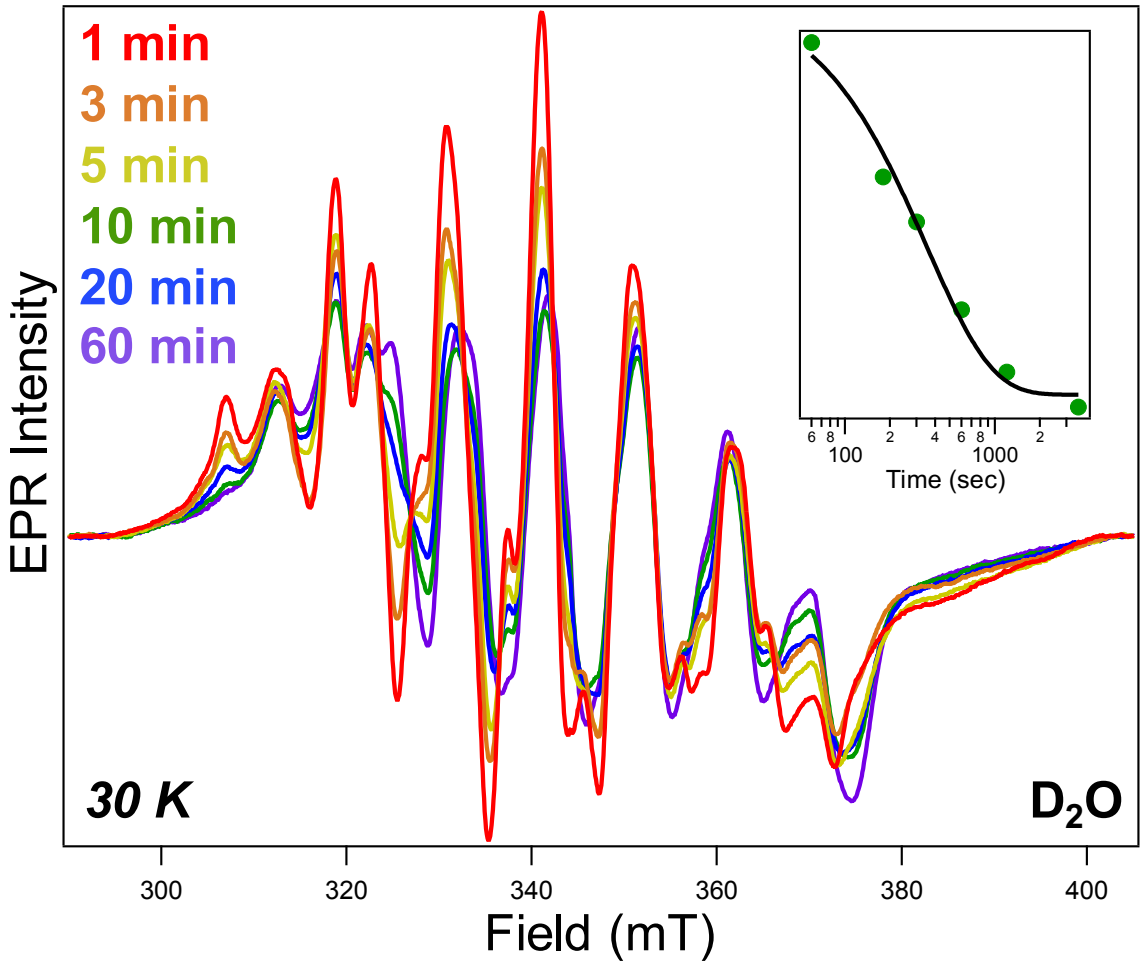

Figure S23. Decay of I_1 in deuterated buffer collected at 30 K, *(inset)* decay kinetics monitored at ~307 with best fit to single exponential shown.

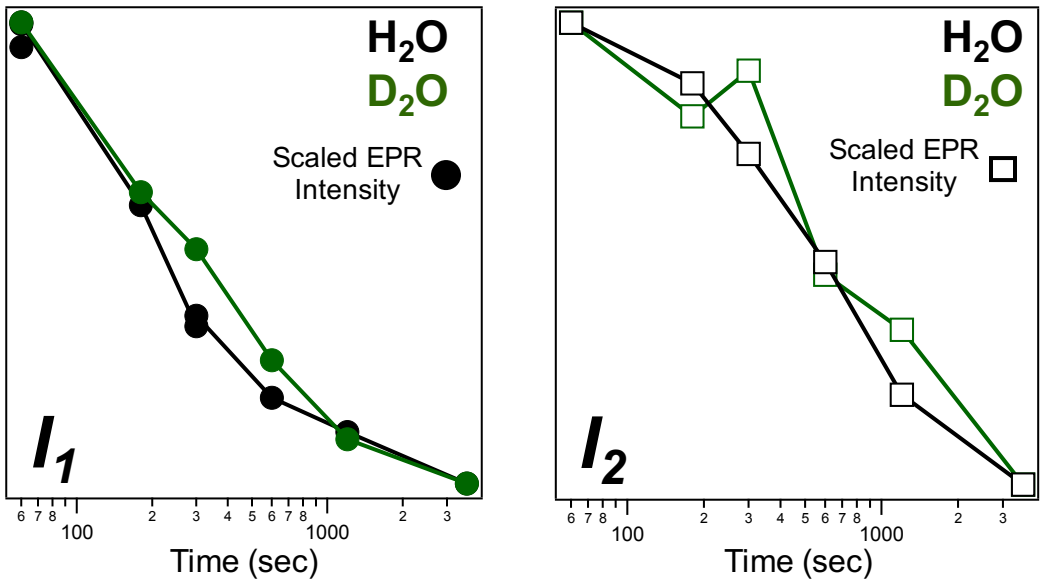

Figure S24. Isotope effects on the kinetic profiles of each intermediate observed via EPR.

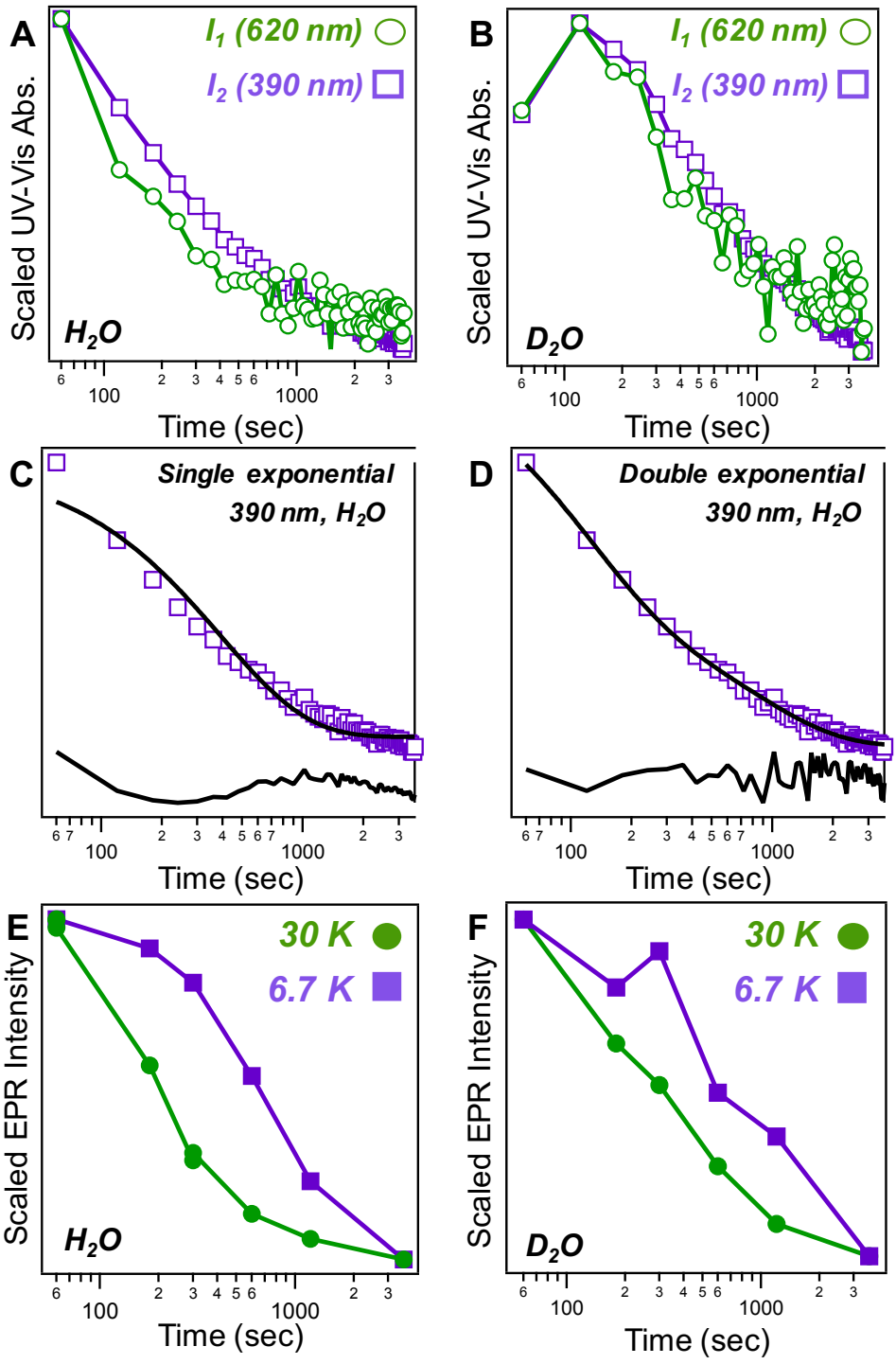

Figure S25. Comparison between optical (A-B) and EPR (E-F) kinetic profiles for distinct intermediates in both protiated and deuterated buffers. In both methods, the decay of I_1 occurs at a faster rate than that of I_2. Decay of I_2 and best fit shown using a single (C) and double (D) exponential function. Residuals for each fit shown below data.

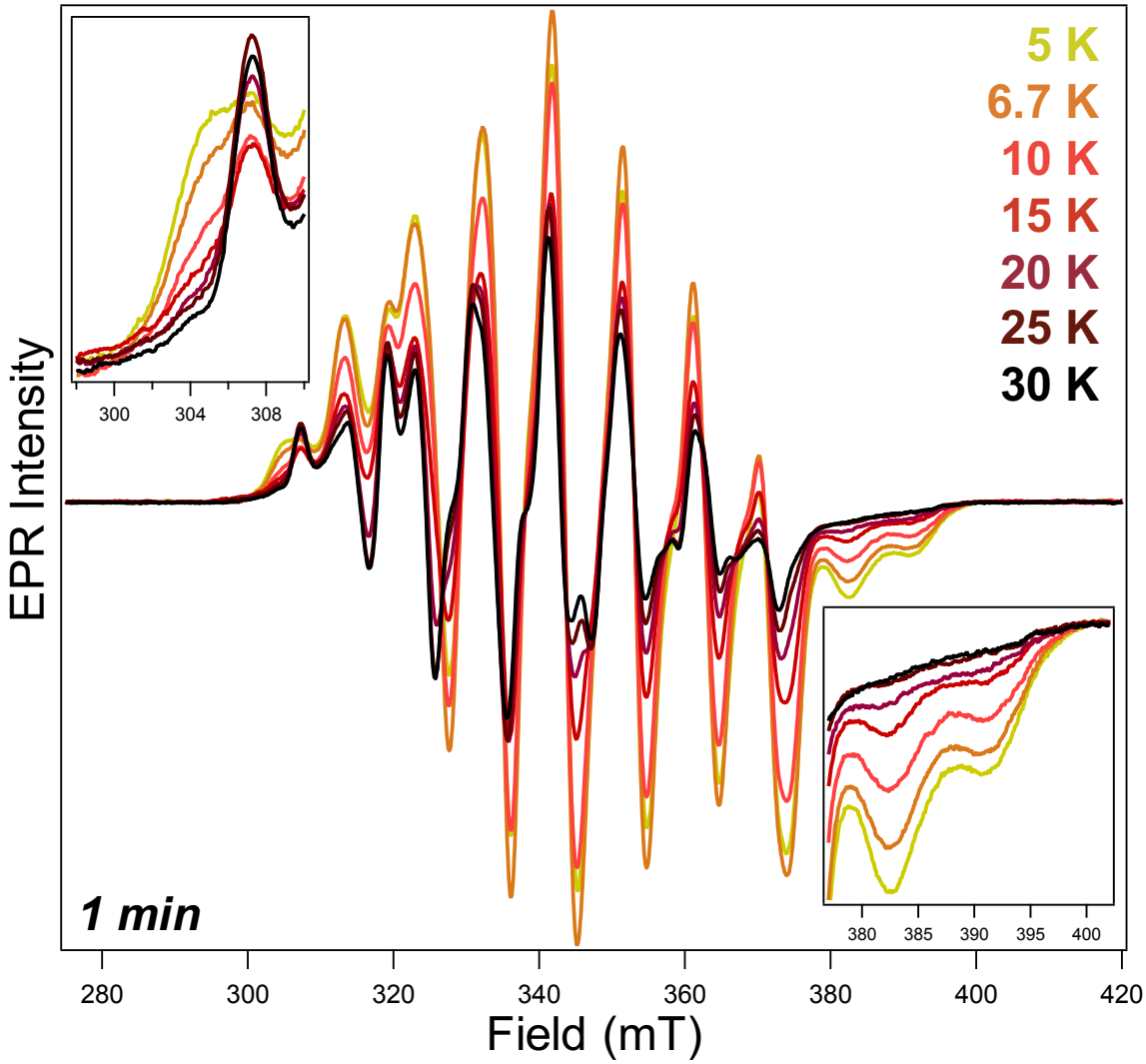

Figure S26. Variable temperature CW X-band EPR spectra of Mn/Fe R2lox hand-quenched at 1 min. Differential relative intensities in low-field signals (*top inset*) show the 307.3 mT species, previously seen only in shorter time points, becoming more intense at higher temperatures. This suggests a slower relaxation time for this species. The 304.8 mT signal shows an approximately inverse temperature dependence, consistent with rapid relaxation rates. The high-field features (*bottom inset*) display a temperature dependence similar to that of the 304.8 mT low-field signal, providing evidence that these signals originate from the same species.

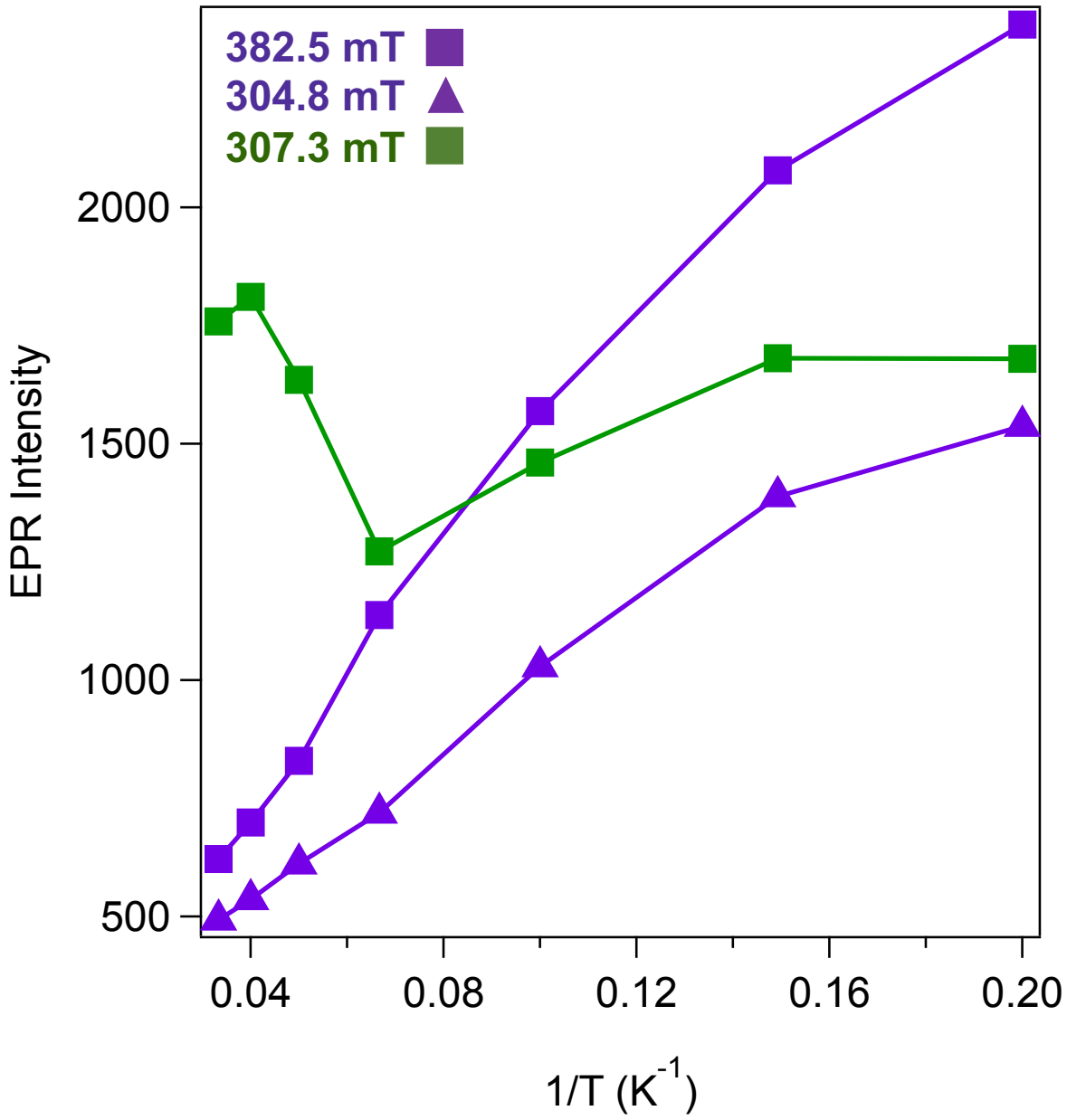

Figure S27. Temperature dependence on EPR intensities of spectral features of intermediate species. Both low- (Δ) and high- (□) field features seen in the broad EPR-active species (I_2) exhibit Curie-like behavior and increase linearly with inverse temperature (purple). Low-field (□) feature of narrow EPR-active species (I_1) does not display a linear dependence on the inverse of temperature (green).

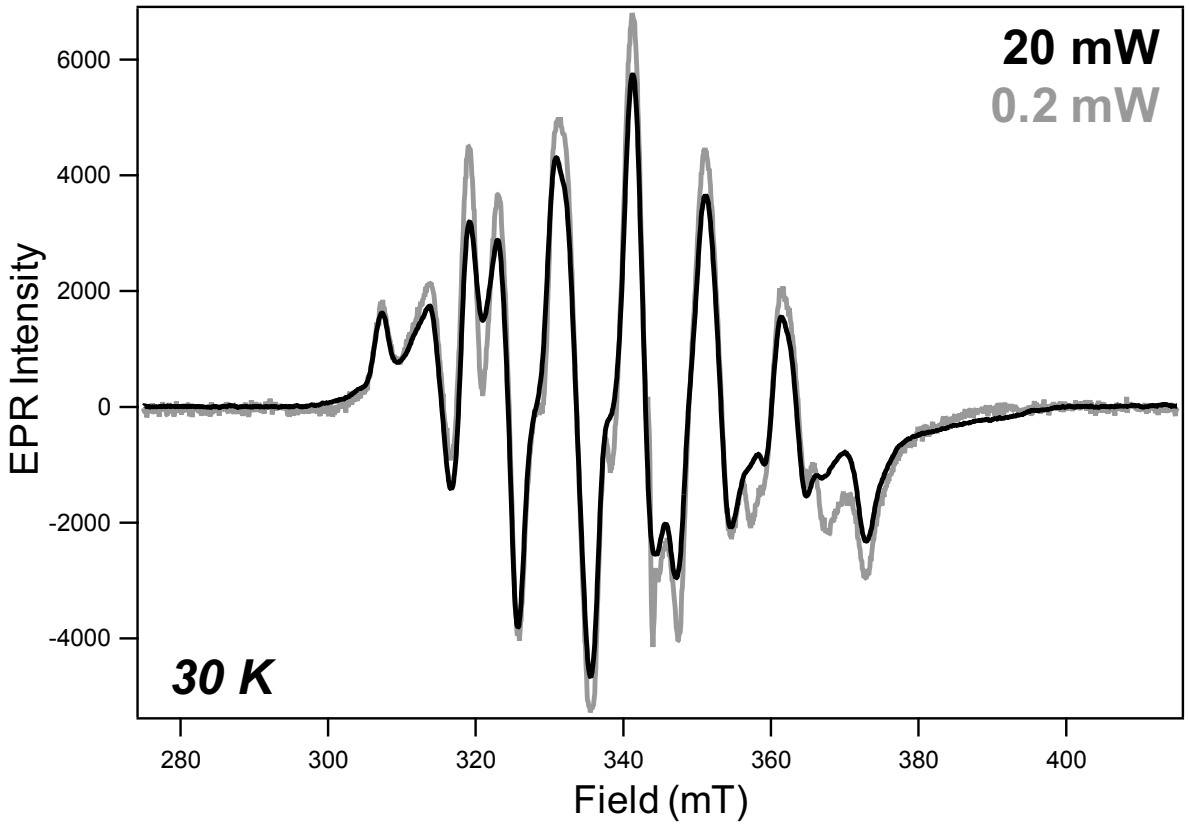

Figure S28. Power dependence of EPR spectrum of I_1 at 30 K. Signals were scaled appropriately (by $P^{1/2}$) to account for different absolute signal intensities.

Supplemental References:

(1) Kutin, Y., Srinivas, V., Fritz, M., Kositzki, R., Shafaat, H. S., Birrell, J., Bill, E., Haumann, M., Lubitz, W., Högbom, M., Griese, J. J., and Cox, N. (2016) Divergent assembly mechanisms of the manganese/iron cofactors in R2lox and R2c proteins. *J. Inorg. Biochem. 162*, 164–177.
(2) Rajakovich, L. J., Nørgaard, H., Warui, D. M., Chang, W., Li, N., Booker, S. J., Krebs, C., Bollinger, J.M., Jr., and Pandelia, M.-E. (2015) Rapid reduction of the diferric-peroxyhemiacetal intermediate in aldehyde-deformylating oxygenase by a cyanobacterial ferredoxin: evidence for a free-radical mechanism. *J. Am. Chem. Soc. 137*, 11695–11709.
(3) Shafaat, H. S., Griese, J. J., Pantazis, D. A., Roos, K., Andersson, C. S., Popović-Bijelić, A., Gräslund, A., Siegbahn, P. E. M., Neese, F., Lubitz, W., Högbom, M., and Cox, N. (2014) Electronic structural flexibility of heterobimetallic Mn/Fe cofactors: R2lox and R2c proteins. *J. Am. Chem. Soc. 136*, 13399–13409.
(4) Banerjee, R., Meier, K. K., Münck, E., and Lipscomb, J. D. (2013) Intermediate P* from soluble methane monooxygenase contains a diferrous cluster. *Biochemistry 52*, 4331–4342.
(5) Bollinger, J.M., Jr., Edmondson, D. E., Huynh, B. H., Filley, J., Norton, and Stubbe, J. (1991) Mechanism of assembly of the tyrosyl radical-dinuclear iron cluster cofactor of ribonucleotide reductase. *Science 253*, 292–298.
(6) Larsson, A., and Sjöberg, B. M. (1986) Identification of the stable free radical tyrosine residue in ribonucleotide reductase. *EMBO J. 5*, 2037–2040.